Grazing-incidence small-angle x-ray scattering from dense packing of islands on surfaces: Development of distorted wave Born approximation and correlation between particle sizes and spacing

Rémi Lazzari,[1,*] Frédéric Leroy,[2,†] and Gilles Renaud[3,‡]

[1]*Institut des NanoSciences de Paris, Universités Pierre et Marie Curie (Paris 6) et Denis Diderot (Paris 7), CNRS UMR 7588, Campus Boucicaut, 140 Rue de Lourmel, 75015 Paris, France*

[2]*Centre de Recherche en Matière Condensée et NanoSciences, CNRS UPR 7281, Campus de Luminy Case 913, 13288 Marseille Cedex 09, France*

[3]*Commissariat à l'Energie Atomique, Département de Recherche Fondamentale sur la Matière Condensée, Service de Physique des Matériaux et Microstructures, Nanostructures et Rayonnement Synchrotron, 17 Avenue des Martyrs, F-38054 Grenoble Cedex 9, France*

(Received 15 September 2006; revised manuscript received 27 April 2007; published 11 September 2007)

This paper is devoted to the analysis methodology of grazing-incidence small-angle x-ray scattering from dense assemblies of islands on a surface. To interpret the experimental data for increasing coverage, (i) the distorted wave Born approximation (DWBA) formalism has been extended to include the exact profile of electronic density, i.e., the fuzziness of the interface, and (ii) the scaling of the Voronoï cell size of each particle with its size has been introduced in the scattering formalism. Multiple scattering effects in the perpendicular direction, i.e., along the emergence angle, are treated within the DWBA using the full perpendicular profile of refraction index as a reference state of the perturbation formalism and not simply the bare substrate. Thus, the average along the surface of the perturbation due to the particles or the holes in between is zero. It is shown that the concept of island form factor is still valid and includes, in a continuous integral, scattering events from upward to downward propagating waves (and vice versa) in the graded interface. Contrary to the case of multiple scattering on the bare substrate, the shape of Yoneda's peak as well as the location and sharpness of the perpendicular interference fringes depend on the coverage for monodisperse particles, or more generally, on the embedding profile of refraction index. In the parallel direction, i.e., along the surface plane, a one dimensional model based on the paracrystal is proposed to include correlations between the size and the spacing of the particles. In this model, the interplay between coherent and incoherent scattering can lead to a hollow of scattered intensity between the specular rod and the correlation peak, as experimentally observed. This size-spacing correlation approximation goes beyond the commonly used approximations of scattering from a dense collection of particles, i.e., (i) the decoupling approximation characterized by a random disorder and by a too intense incoherent scattering and (ii) the convenient local monodisperse approximation which relies on a description of the scattering system as a set of monodisperse domains, which is not physically sound in many cases. The three approximations are compared on a physically relevant case. In a following experimental paper [R. Lazzari *et al.*, Phys. Rev. B **76**, 125412 (2007)], these models are applied to the analysis of the $Au/TiO_2(110)$ growth mode.

DOI: 10.1103/PhysRevB.76.125411 PACS number(s): 61.10.Dp, 61.10.Kw, 81.15.Aa, 68.55.Ac

I. INTRODUCTION

The field of crystalline growth on surfaces has benefited for four decades from a huge amount of theoretical and experimental work. Understanding the elementary and prevailing mechanisms involved during the nucleation, growth, and coalescence of a thin film made of nanoparticles relies on the study of its morphology at different stages of deposition, in particular, as function of temperature and evaporation flux. These morphological observations are interpreted with the help of suitable theories or numerical simulations.[2–4] However, even if scanning near field microscopies have been a breakthrough in *in situ* studies of growth, real space observations suffer from slowness, sampling limits, and artifacts. These drawbacks can be overcome with x-ray scattering using the grazing-incidence geometry. Quite recently, it has been shown that the grazing-incidence small-angle x-ray scattering (GISAXS) technique[5,6] can be applied to follow the growth of nanoparticles *in situ* and in the ultrahigh vacuum environment. However, obtaining reliable morphological information on the islands implies a complex data analysis in reciprocal space because multiple scattering effects due to the grazing incidence[7,8] and interference effects in dense system of particles have to be taken into account. The usual available models developed to analyze the data are based on two approximations: the distorted wave born approximation (DWBA) with the substrate surface as a reference state for the wave propagation[9] and the local monodisperse approximation (LMA)[10–14] stating that the island layer consists of monodisperse domains. These two approximations fail for dense system of particles as it has been evidenced by applying them to many GISAXS data sets.[15] The topic of this work is to develop a model that can improve the data analysis.

Up to now, the analysis of GISAXS from nanoparticles on surfaces[5,9,15–17] was performed using the DWBA with the substrate surface as reference state. In particular and at variance to the Born approximation, for one island on a bare substrate,[9] four scattering events involving the reflection-refraction of the incident or scattered wave on the bare substrate appear in the scattering cross section. However, upon increasing the packing of islands on the surface, that is to

say, the electronic density above the surface, the perturbation on the incident and scattered wave field propagations becomes larger and larger. As the growth proceeds, the particles can no longer be treated as isolated scatterers.[16] The main signature in the GISAXS patterns[5,15,17] is a progressive rounding and shift of Yoneda's peak with increasing film thickness going from a refraction effect of the bare substrate toward that of the deposited material. It was found that this phenomenon could be roughly simulated by adjusting the refractive index of the substrate[15] in the theory of scattering by an isolated particle.[9] However, such a trick can lead to values quite different from tabulated ones[18] with a shift of the location of perpendicular interference fringes of the form factor. The right way of doing it is to start the perturbation formalism of DWBA from the exact averaged perpendicular profile of refraction index; this leads to a translationally invariant reference system with a null average of the perturbation along the surface. This extension to graded interface (i) was already suggested in the literature, in particular, for a general profile[19,20] or for special tractable profiles[21] such as tangent hyperbolicus, and (ii) is in line with DWBA higher order expansion of the integral equation of scattering[22,23] from multilayers[19,24–30] or from thin polymer films with lamellar structures.[31] However, such a model has neither been generalized to the case of islands nor applied to the analysis of a full set of experimental data.

The scattering from a dense collection of particles differs significantly from that of isolated particles not only in the perpendicular direction but also in the parallel one. This quite general problem of small-angle scattering from concentrated systems of particles[10,32] is due to the intrinsic lack of knowledge of all the partial interference functions that come into play in the buildup of the scattered intensity. A solution can be found in the theory of liquid state which aims at determining the thermodynamic equilibrium properties of liquids.[33,34] One of the scarce solutions of scattering from polydispersed systems was given by Vrij and coworker[35–37] on a three dimensional (3D) system of interacting hard spheres treated in the Percus-Yevick approximations.[33] Applications to data analysis can be found in Refs. 12 and 38. Gazzillo *et al.*[14] proposed a model, called scaling approximation (SA), to bypass the resolution of the integral equation of liquid theory and to evaluate the scattering from polydispersed particles. SA is based on the hypothesis of a conformal pair interaction potential, a conformal mixture, and a scaling approximation of all the radial distribution functions. SA reduces the problem to the knowledge of the structure factor of one pure state. Satisfactory performance was found with the hard-core potential as compared to Vrij's results and with the Lennard-Jones' one as compared to molecular dynamics simulations. However, at variance to mixture of liquids or colloids fluids, the islands grown on surface by thermal evaporation do not interact through a potential. The growth is often a process far from equilibrium[3,4,39] and the particle radial distribution functions result from a complex interplay between all the elementary phenomena involved during nucleation, growth, and coalescence.[2]

Small-angle scattering experimentalists often prefer to resort to some "cruder" approximations than using complex theory of liquids. The first one, known as the decoupling approximation (DA),[10,32,40–42] neglects all these correlations;it leads to a unique interference function and to a broad incoherent scattering term centered at the origin and arising from the particle size and shape distributions. The first numerical calculations and successful applications with DA were performed by Kotlarchyk and Chen[42] on neutron scattering from polydisperse colloids in solution. The second one, the so-called local monodisperse approximation,[10–14] assumes an incoherent scattering from monodisperse domains and gives rise to a very simple cross section as the average over the domains of the product of the form factor times an interference function. The LMA underlying hypothesis on the morphology is not valid for most of the particle systems; however, some successful results have been obtained for the analysis of scattering of metallic precipitates in a matrix.[12,38,43] As long as the high wave vector transfer range is under concern, all the approximations give the same results as the scattering is dominated by the mean particle form factor. However, interference effects between the wave scattered by each particle concentrate the intensity in the so-called correlation peak. Unfortunately, because of signal-to-noise ratio, the fit of experimental data is often dominated by this preeminent feature.

Revenant *et al.*[15] have applied the DA and LMA approximations to GISAXS measurements on Pd/MgO(001). It was concluded that the DA overestimates the signal close to the specular rod, while the LMA satisfactorily reproduces the correlation peak using an *ad hoc* interference function. It was highlighted, using transmission electron microscopy plane views, that the sizes of neighboring particles are not correlated (at variance to the LMA hypothesis), while a strong correlation between the diameter of the island and the distance to its first neighbor shows up. It was suggested that this "hard-core-type" effect yields a decrease of the scattered intensity close to the specular rod (contrary to DA) when calculating the expected scattering from real space images. Even though the general formulation of such a problem of correlation between scatterers can be found in standard text books of crystallography,[40,44] a practical application to small-angle scattering from 3D particles is desirable. For that purpose, a one dimensional (1D) model[45] of correlated 3D particles is proposed in order to reproduce GISAXS data.

This paper is organized as follows. Section II A focuses on the calculation of the scattering cross section from a graded interface made of islands within the framework of the DWBA. The concept of particle form factor is generalized; the dramatic influence of particle density (or more generally the embedding gradient of index of refraction) on Yoneda's peak shape and on the location and degree of sharpness of the out-of-plane scattering lobes is illustrated. Owing to the decoupling between the parallel and perpendicular directions, Sec. III deals only with the problem of correlation between the size of the scatterers and their spacing along the substrate plane. A one dimensional formalism of scattering by 3D particle derived from the paracrystal theory[41,46–48] is proposed. The application to the experimental case of GISAXS from Au islands on TiO_2(110) will be described in a forthcoming paper (Ref. 1).

II. X-RAY SCATTERING FROM ISLANDS AT GRAZING INCIDENCE: THEORETICAL BACKGROUND

A. Distorted wave Born approximation scattering cross section from a graded interface

The scattering cross section from a collection of islands on a substrate is calculated within the formalism of the distorted wave Born approximation.[7,8,25,49] On a fundamental point of view, DWBA cross sections can be obtained from the reciprocity theorem as illustrated in Refs. 50 and 51. This semidynamical treatment allows the separation of the scattering process itself, which is treated within the kinematic approximation, from the intense specular reflectivity of the surface observed close to the angle of total external reflection. The DWBA is thus a perturbation formalism applied to a wave field that includes the dynamical effect of reflection-refraction at interfaces; the unperturbed state is generally taken as the Fresnel wave field, which is analytical for flat interfaces. For an isolated island, taking as a reference the flat substrate, Rauscher *et al.*[9] have shown that the cross section involves an interference between four scattering processes that include, or not, reflections on the substrate of the incident or scattered wave. In the obtained scattering pattern, Yoneda's peak comes from the interplay between the four events and the Fresnel reflection coefficients.

However, for a densely packed collection of particles, once scattered, a wave may be (i) rescattered, in particular, in the specular direction, and (ii) attenuated within the layer, like the incident wave. This is all the more true when the path of the wave inside the island layer is large, i.e., for an emergence angle close to the critical angle. Moreover, before scattering, the incident wave feels a mirage effect in the gradient of refractive index that modifies its amplitude. For disordered systems where no special spatial frequency (i.e., diffraction direction by periodic roughness) in the substrate plane shows up, secondary scattering with parallel wave vector transfer has a negligible cross section even under grazing angles. Thus, the incident and scattered waves see only the perpendicular density profile averaged over the surface if the projected coherence length of the beam is larger than the characteristic spatial frequency of the roughness. Generally speaking, a perturbation formalism is all the more valid when the perturbation is small; in other words, the unperturbed state should be as close as possible to the real state. As a consequence, the DWBA is expected to be improved compared to flat interfaces as a reference state if the starting point of wave fields includes the dynamical effect of reflection induced by the full perpendicular profile of density. By doing so, the roughness perturbation induced by the islands is null on average in the direction perpendicular to the substrate. Even though the emphasis is put on islands, the concepts developed in the following are also valid for other kinds of surface roughnesses.

The DWBA method starts from the Helmholtz propagation equation for the electric field amplitude $\Psi(\mathbf{r})$; the latter is reduced to a scalar one as the polarization effects can be safely ignored at small angles:[21]

$$[\nabla^2 + k_0^2 n^2(\mathbf{r})]\Psi(\mathbf{r}) = 0, \tag{2.1}$$

where $k_0 = 2\pi/\lambda$ is the vacuum wave vector modulus. The local index of refraction $n^2(\mathbf{r})$,

$$n^2(\mathbf{r}) = n_0^2(z) + (n_i^2 - 1)\sum_j \mathcal{S}_j(\mathbf{r}_\parallel - \mathbf{r}_{\parallel,j}, z), \tag{2.2}$$

includes the index of refraction of the substrate and vacuum,

$$n_0(z) = \begin{cases} 1 & \text{if } z > 0 \\ n_s = 1 - \delta_s - i\beta_s & \text{if } z < 0, \end{cases} \tag{2.3}$$

and that $n_i = 1 - \delta_i - i\beta_i$ of the layer of islands of shapes $\mathcal{S}_j(\mathbf{r})$ [$\mathcal{S}_j(\mathbf{r}) = 0$ or 1 outside or inside the island, respectively] located at $\mathbf{r}_{\parallel,j}$ on the substrate surface. To include in the perturbation formalism the perpendicular average index of refraction $\tilde{n}_0(z)$, $n^2(\mathbf{r})$ is rewritten as

$$n^2(\mathbf{r}) = \tilde{n}_0^2(z) + \delta n^2(\mathbf{r}_\parallel, z), \tag{2.4}$$

where

$$\tilde{n}_0^2(z) = \begin{cases} 1 & \text{if } z > t \\ \tilde{n}_l^2(z) = 1 + [(n_i^2 - 1)/S]\displaystyle\int_S \sum_j \mathcal{S}_j(\mathbf{r}_\parallel - \mathbf{r}_{\parallel,j}, z)\, d\mathbf{r}_\parallel & \text{if } 0 < z < t \\ n_s^2 & \text{if } z < 0, \end{cases} \tag{2.5}$$

t being the thickness of the island layer and S the sample surface with $S \to \infty$. The perturbation is thus brought for each z level by the departure from $\tilde{n}_l^2(z)$ induced by the matter, i.e., the islands or the holes in between:

$$\delta n^2(\mathbf{r}_\parallel, z) = [n_i^2 - \tilde{n}_l^2(z)]\sum_j \mathcal{S}_j(\mathbf{r}_\parallel - \mathbf{r}_{\parallel,j}, z) + [1 - \tilde{n}_l^2(z)]\mathcal{S}_{hole}(\mathbf{r}_\parallel, z). \tag{2.6}$$

The shape factor for the vacuum between islands is nothing else but the inverse fingerprint of the islands $\mathcal{S}_{hole}(\mathbf{r}_\parallel, z) = \Theta(z) - \Theta(z-t) - \Sigma_j \mathcal{S}_j(\mathbf{r}_\parallel - \mathbf{r}_{\parallel,j}, z)$, $\Theta(z)$ being the step function [$\Theta(z) = 0$ for $z < 0$ and $\Theta(z) = 1$ for $z > 0$]. Thus,

$$\delta n^2(\mathbf{r}_\parallel, z) = \delta n_1^2(\mathbf{r}_\parallel, z) + \delta n_2^2(z) = [n_i^2 - 1]\sum_j \mathcal{S}_j(\mathbf{r}_\parallel - \mathbf{r}_{\parallel,j}, z) + [1 - \tilde{n}_l^2(z)][\Theta(z) - \Theta(z-t)]. \tag{2.7}$$

As no parallel dependence appears in $\tilde{n}_0(z)$, the Fresnel wave field solution without perturbation for a unit incident wave in vacuum $\mathbf{k} = (\mathbf{k}_\parallel, k_{z,0})$ is made of upward and downward propagating waves:

$$\Psi_0(\mathbf{r},\mathbf{k}) = e^{i\mathbf{k}_\parallel\cdot\mathbf{r}_\parallel}\begin{cases} \tilde{A}_0^+ e^{ik_{z,0}z} + e^{-ik_{z,0}z} & \text{for } z > t \\ \tilde{A}_1^+(z)e^{ik_{z,1}(z)z} + \tilde{A}_1^-(z)e^{-ik_{z,1}(z)z} & \text{for } 0 < z < t \\ \tilde{A}_2^- e^{-ik_{z,2}z} & \text{for } z < 0. \end{cases} \tag{2.8}$$

The perpendicular components of the wave vector transfer are $k_{z,0}(z)=-\sqrt{k_0^2-k_\parallel^2}$ in vacuum, $k_{z,1}(z)=-\sqrt{\tilde{n}_l^2(z)k_0^2-k_\parallel^2}$ inside the layer, and $k_{z,2}(z)=-\sqrt{n_s^2k_0^2-k_\parallel^2}$ inside the substrate. In the graded island interface, the amplitudes $\tilde{A}_1^\pm(z)$ vary continuously; knowing the profile of index of refraction, they can be computed through differential equations or through a matrix formalism (see Sec. II B).

The far field expansion of the retarded Green's function[52] associated with the unperturbed Helmholtz propagation equation [Eq. (2.1)] reads

$$G(\mathbf{r},\mathbf{r}',k_0^2) \sim -k_0^2\frac{e^{-ik_0r}}{4\pi r}\Psi_0(\mathbf{r}',-\mathbf{k}_f). \tag{2.9}$$

By expanding to first order in perturbation the integral solution of the scattering equation for an incoming plane wave $\mathbf{k}_i$, the total solution $\Psi(\mathbf{r})$ reads

$$\begin{aligned}\Psi(\mathbf{r}) &\simeq \Psi_0(\mathbf{r},\mathbf{k}_i) + \Psi_{sc}(\mathbf{r},\mathbf{k}_i,\mathbf{k}_f) \\ &= \Psi_0(\mathbf{r},\mathbf{k}_i) + k_0^2\frac{e^{-ik_0r}}{4\pi r}\int d\mathbf{r}'\Psi_0(\mathbf{r}',-\mathbf{k}_f)\delta n^2(\mathbf{r}') \\ &\quad\times\Psi_0(\mathbf{r}',\mathbf{k}_i)\end{aligned} \tag{2.10}$$

As the incident beam coherence is limited (angular and wavelength spreads) and the detector acceptance is finite, the measurable intensity is given by an incoherent sum of the intensities stemming for the coherently illuminated domains A_{coh}, i.e., $\langle|\Psi(\mathbf{r})|^2\rangle_S$. Moreover, it is assumed that A_{coh} is sufficiently large so that the system presents the same statistical properties over each domain A_{coh}. This spatial average denoted $\langle\cdots\rangle_A$ is equivalent to a configuration average $\langle|\Psi(\mathbf{r})|^2\rangle$ over many realizations of the random ergodic process, that is, the surface morphology.[50] As $\Psi_{sc}(\mathbf{r})$ is a fluctuating quantity,

$$\begin{aligned}\langle|\Psi(\mathbf{r})|^2\rangle &= |\Psi_0(\mathbf{r},\mathbf{k}_i) + \langle\Psi_{sc}(\mathbf{r},\mathbf{k}_i,\mathbf{k}_f)\rangle|^2 + \langle|\Psi_{sc}(\mathbf{r},\mathbf{k}_i,\mathbf{k}_f)|^2\rangle \\ &\quad - |\langle\Psi_{sc}(\mathbf{r},\mathbf{k}_i,\mathbf{k}_f)\rangle|^2.\end{aligned} \tag{2.11}$$

The choice of the graded interface as the unperturbed state yields $\langle\Psi_{sc}(\mathbf{r},\mathbf{k}_i,\mathbf{k}_f)\rangle \sim \langle\delta n^2(\mathbf{r}_\parallel,z)\rangle = 0$. Thus, following Ref. 7, the specular scattering cross section per sample surface unit (or the so-called coherent scattering or reflectivity) is given by

$$\left(\frac{d\sigma}{d\Omega}\right)_{coh} = Sk_0^2\sin^2(\alpha_f)|A_0^+(k_{iz,0})|^2\delta(\mathbf{q}_\parallel), \tag{2.12}$$

where $\mathbf{q}_\parallel=\mathbf{k}_{f\parallel}-\mathbf{k}_{i\parallel}$ is the in-vacuum wave vector transfer parallel to the surface. An experimental broadening of the specularly reflected beam ($k_{fz,0}=-k_{iz,0}$, $\mathbf{q}_\parallel=0$) due to finite beam coherence (beam divergence, detector acceptance, sample macroscopic curvature) is, of course, expected. The collision theory[52] gives the incoherent differential scattering cross section as

$$\left(\frac{d\sigma}{d\Omega}\right)_{incoh} = \frac{r^2}{S}\langle|\Psi_{sc}(\mathbf{r},\mathbf{k}_i,\mathbf{k}_f)|^2\rangle. \tag{2.13}$$

As $\delta n^2(\mathbf{r})$ [Eq. (2.7)] consists of two terms among which $\delta n_2^2(z)$ does not vary along the surface, the same reasoning as in Eq. (2.11) yields

$$\begin{aligned}\langle|\Psi_{sc}(\mathbf{r},\mathbf{k}_i,\mathbf{k}_f)|^2\rangle &= |\Psi_{sc}[\delta n_2^2(z)] + \langle\Psi_{sc}[\delta n_1^2(z,\mathbf{r}_\parallel)]\rangle|^2 \\ &\quad + \langle|\Psi_{sc}[\delta n_1^2(z,\mathbf{r}_\parallel)]|^2\rangle - |\langle\Psi_{sc}[\delta n_1^2(z,\mathbf{r}_\parallel)]\rangle|^2.\end{aligned} \tag{2.14}$$

Upon inserting the definition [Eq. (2.5)] of the gradient of dielectric constant in the previous equation, it appears that $\Psi_{sc}[\delta n_2^2(z)]+\langle\Psi_{sc}[\delta n_1^2(z,\mathbf{r}_\parallel)]\rangle \sim \delta n_2^2(z)+\langle\delta n_1^2(z,\mathbf{r}_\parallel)\rangle = 0$. Moreover, the last term of Eq. (2.14) that involves the diffuse scattering on the average profile of refraction index contributes only close to $\mathbf{q}_\parallel \simeq 0$; its $q_\parallel$ width is driven by the beam and sample coherence length. As only GISAXS measurements are under concern, it will be omitted in the following. After having noticed that the perturbation potential $\delta n_1^2(z,\mathbf{r}_\parallel)$ of Eq. (2.5) acts only for $0<z<t$, the introduction of the Fresnel wave field expression of Eq. (2.8) into Eqs. (2.10)–(2.13) leads to the following result for the incoherent scattering cross section (not too close to $q_\parallel=0$) from a plane wave $\mathbf{k}_i$ into a plane wave $\mathbf{k}_f$ per surface unit:

$$\left(\frac{d\sigma}{d\Omega}\right)_{incoh} \simeq \frac{\rho_S k_0^4|n_i^2-1|^2}{16\pi^2}\langle\Phi(\mathbf{q}_\parallel,k_{iz},k_{fz})\rangle$$

$$\text{with } \Phi(\mathbf{q}_\parallel,k_{iz},k_{fz}) = \frac{1}{N}\left|\sum_j \mathcal{F}_j(\mathbf{q}_\parallel,k_{iz},k_{fz})e^{i\mathbf{q}_\parallel\cdot\mathbf{r}_{\parallel,j}}\right|^2, \tag{2.15}$$

where ρ_S is the density of particles and N the total number of scatterers. The separation between the parallel and perpendicular scattering directions allows us to introduce the DWBA effective form factor of one island:

$$\begin{aligned}\mathcal{F}_j(\mathbf{q}_\parallel,k_{iz},k_{fz}) &= \int d\mathbf{r}_\parallel e^{i\mathbf{r}_\parallel\cdot\mathbf{q}_\parallel}\int dz\mathcal{S}_j(\mathbf{r}_\parallel,z) \\ &\quad\times\{\tilde{A}_1^-[k_{iz,1}(z)]\tilde{A}_1^-[-k_{fz,1}(z)]e^{i[+k_{fz,1}(z)-k_{iz,1}(z)]z} \\ &\quad+\tilde{A}_1^+[k_{iz,1}(z)]\tilde{A}_1^-[-k_{fz,1}(z)]e^{i[+k_{fz,1}(z)+k_{iz,1}(z)]z} \\ &\quad+\tilde{A}_1^-[k_{iz,1}(z)]\tilde{A}_1^+[-k_{fz,1}(z)]e^{i[-k_{fz,1}(z)-k_{iz,1}(z)]z} \\ &\quad+\tilde{A}_1^+[k_{iz,1},(z)]\tilde{A}_1^+[-k_{fz,1}(z)]e^{i[-k_{fz,1}(z)+k_{iz,1}(z)]z}\}.\end{aligned} \tag{2.16}$$

The introduced particle form factor is neither a simple Fourier transform of its shape (as found in the Born approximation) nor a sum of four scattering terms including only the reflection of the incident or scattered waves on the substrate as it was found in Ref. 9 by taking the flat substrate as the unperturbed state. Instead, $\mathcal{F}_j(\mathbf{q}_\parallel,k_{iz},k_{fz})$ includes scattering from upward (downward) to upward (downward) propagating waves inside the graded interface. Obviously, for isolated

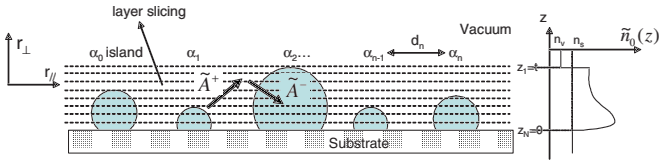

FIG. 1. (Color online) Schematic drawing of the island layer. $\tilde{n}_0(z)$ is obtained upon averaging the refraction index (islands and vacuum holes in between) in each slice. In each slice, the upward $\tilde{A}^+(z)$ and downward $\tilde{A}^-(z)$ propagating waves are computed recursively. The form factor $\mathcal{F}(\mathbf{q}_\parallel, k_{iz}, k_{fz})$ [see Eq. (2.16)] including the wave field propagation inside the layer is used as an input in the size-spacing correlation approximation formula [Eq. (3.14)].

particles, $\tilde{n}_0(z) \simeq n_0(z)$, $k_{z,0} \simeq k_{z,1}$, and $\tilde{A}_1^+ \simeq \tilde{A}_0^+$, $\tilde{A}_1^- = \tilde{A}_0^- = R_F$ (R_F is the Fresnel reflectivity of the substrate): Eq. (10) of Ref. 9 is recovered.

B. Numerical implementation

Let us focus on the calculation of the particle form factor $\mathcal{F}(\mathbf{q}_\parallel, k_{iz}, k_{fz})$ [Eq. (2.16)] embedded in a graded interface (see Fig. 1). Once assumed the island size and shape distributions and the particle in-plane density, the profile of index of refraction can easily be evaluated through Eq. (2.5) as well as the perpendicular component of the incident $k_{iz,1}$ and scattered $k_{fz,1}$ wave vectors. On a practical point of view, a matrix formalism of Abelès' type[50] was used to compute the amplitudes of the upward $\tilde{A}_1^+[-k_{z,1}(z)]$ and downward $\tilde{A}_1^-[-k_{z,1}(z)]$ propagating waves. The graded interface is sliced in N layers, $j=1,\ldots,N$ in the downward direction, starting at the vacuum/layer interface $z=t=z_1$ and ending at the substrate/layer interface $z=0=z_N$. The transition matrix from $A_{1,j}^\pm$ to layer $A_{1,j+1}^\pm$ (Ref. 50) includes the propagation inside the layer and the beam reflection-refraction at interfaces:

$$\begin{bmatrix} A_{1,j}^+ \\ A_{1,j}^- \end{bmatrix} = \begin{bmatrix} p_{j,j+1} e^{i(k_{z,1,j+1}-k_{z,1,j})z_{j+1}} & m_{j,j+1} e^{-i(k_{z,1,j+1}+k_{z,1,j})z_{j+1}} \\ m_{j,j+1} e^{i(k_{z,1,j+1}+k_{z,1,j})z_{j+1}} & p_{j,j+1} e^{-i(k_{z,1,j+1}-k_{z,1,j})z_{j+1}} \end{bmatrix} \times \begin{bmatrix} A_{1,j+1}^+ \\ A_{1,j+1}^- \end{bmatrix}, \tag{2.17}$$

where

$$p_{j,j+1} = \frac{k_{z,1,j} + k_{z,1,j+1}}{2k_{z,1,j}}, \quad m_{j,j+1} = \frac{k_{z,1,j} - k_{z,1,j+1}}{2k_{z,1,j}}. \tag{2.18}$$

The upward propagating wave inside the substrate does not exist and the amplitudes are normalized to a unit incident wave. Thus, the integral over the z variable in Eq. (2.16) is reduced to a discrete sum of the four Fourier transforms for each slice of island. The slicing of the graded interface is chosen linear in index of refraction, thus, in general, nonlinear in the slice thicknesses. The number of slices is of course increased until numerical convergence, whereas the slice Fourier transform is calculated with a desired accuracy through a suitable integration algorithm.

C. Illustrative examples of form factors

The chosen form factor examples correspond to the experimental case of GISAXS from gold islands on TiO_2.[1] In a GISAXS experiment,[6] the scattered intensity is collected as function of the in-plane scattering angle $2\theta_f$ and the out-of-plane one α_f at a constant incident angle α_i. Forgetting the curvature of the Ewald sphere, the latter is related to the parallel $q_\parallel = 2\pi\lambda[\cos(\alpha_f)\sin(2\theta_f)]$ and perpendicular $q_\perp = 2\pi/\lambda[\sin(\alpha_f) + \sin(\alpha_i)]$ wave vector transfers. The chosen wavelength is $\lambda = 0.068\,88$ nm ($E = 18$ keV) and the corresponding indices of refraction are $\delta_i = 9.73 \times 10^{-6}$, $\beta_i = 1.06 \times 10^{-6}$ and $\delta_s = 2.62 \times 10^{-6}$, $\beta_s = 3.02 \times 10^{-8}$, while the critical angle of total external reflection of the substrate is $\alpha_c = 0.131°$. Two different monodisperse shapes have been used: (i) a cylinder of radius $R = 1$ nm and of height $H = 1$ nm and (ii) a full sphere of radius $R = 1$ nm.

1. Coverage effect

Figures 2 and 3 illustrate the result of an increasing packing of islands on the cylinder and sphere form factors, respectively, at various incident angles α_i. The coverage, defined as $\Theta = \rho_S \pi R^2$ (ρ_S being the particle density), is varied from 0 to 50%. $\Theta = 0$ should be understood as the case of an isolated island on a substrate; the corresponding profile of refraction index is a sharp Heaviside function between vacuum and substrate values. Thus, the form factor is computed starting from the Fresnel wave field of the flat substrate according to Ref. 9. The embedding gradient of index corresponds to a constant value for a cylinder or to a parabola for a full sphere (see the inset of Fig. 4, the top value having to be rescaled by the actual coverage). As a matter of comparison, the particle Fourier transform, i.e., the Born term, has been included in figures.

At variance to the form factor of Ref. 9 ($\Theta = 0$), Figs. 2 and 3 show that Yoneda's peak shape and intensity markedly depend on the coverage: its shape gets asymmetric and decreases in intensity upon increasing the coverage, whatever the particle is. This effect is essentially due to the coverage dependent absorption of the evanescent waves. At high coverage, Yoneda's peak is replaced by a broad bump, especially when $\alpha_i \leqslant \alpha_c$.

Figures 2 and 3 also show that the sharpness and location of the fringes of scattering (the so-called Kiessig fringes in reflectivity) vary strongly with coverage all the more when the angles are grazing. However, as expected, the simple Born approximation is recovered for $\alpha_i, \alpha_f \gg \alpha_c$. For the cylinder case, at a coverage of $\Theta = \delta_s / \delta_i = 0.27$, i.e., $\delta_{layer} = \delta_s$ (see $\Theta = 0.3$ on Fig. 2), the island layer behaves like the substrate in terms of refraction. Thus, if the absorption is ignored, $k_{z,1} = k_{z,2}$, $\tilde{A}_1^+(z) = 0$, $\tilde{A}_1^-(z) = \tilde{A}_2^-(z)$, and

$$\mathcal{F}(\mathbf{q}_\parallel, k_{iz}, k_{fz}) = \tilde{A}_2^-[k_{iz,2}]\tilde{A}_2^-[-k_{fz,2}] \times \int d\mathbf{r}_\parallel e^{i\mathbf{r}_\parallel \cdot (\mathbf{q}_\parallel + k_{fz,2} - k_{iz,2})} \mathcal{S}(\mathbf{r}) d\mathbf{r}. \tag{2.19}$$

$\mathcal{F}(\mathbf{q}_\parallel, k_{iz}, k_{fz})$ appears as the form factor of a particle buried under the substrate surface, and its value is nothing else but the Fourier transform of the particle shape without any blur-

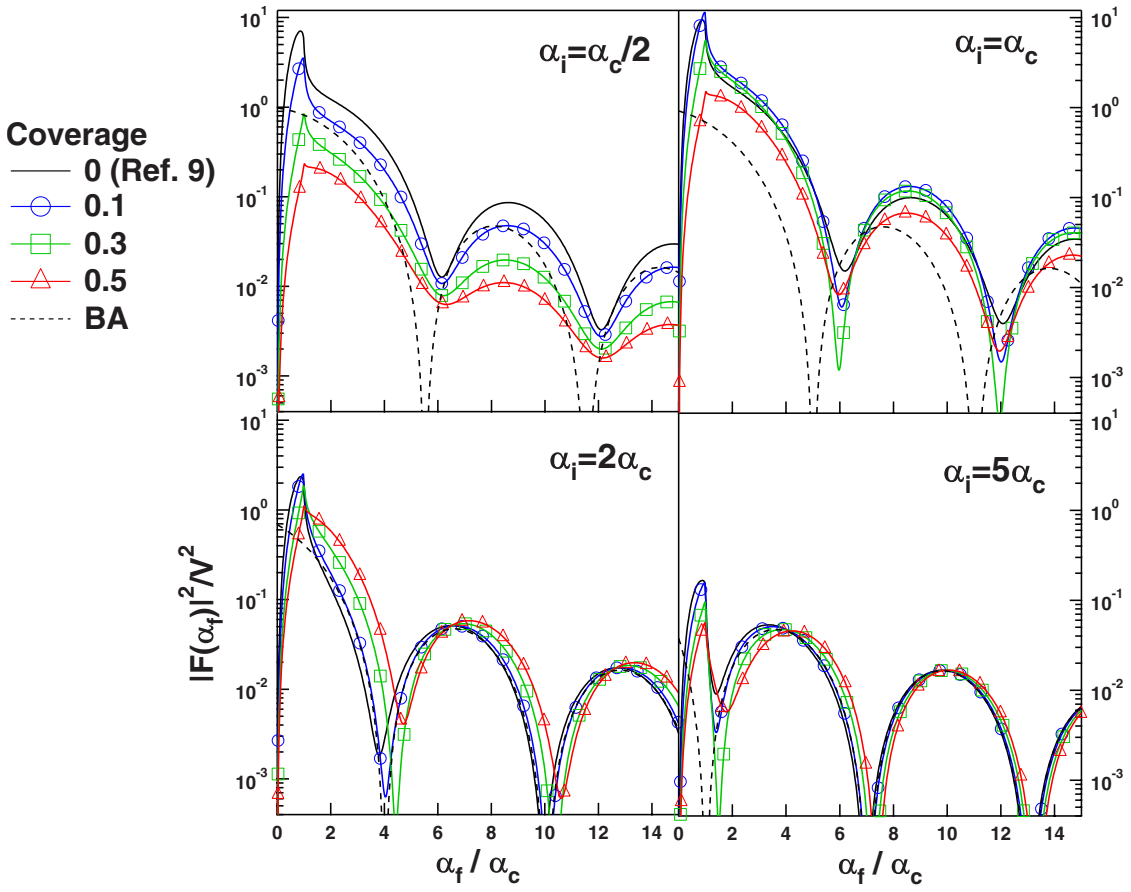

FIG. 2. (Color online) Modulus squared of a cylinder form factor $|\mathcal{F}(\mathbf{q}_\parallel=0, k_{iz}=-k_0 \sin(\alpha_i), k_{fz}=k_0 \sin(\alpha_f))|^2$ [see Eq. (2.16)] for increasing coverage Θ at various incident angles α_i. The dashed curve corresponds to the classical Born term, while $\Theta=0$ is the DWBA form factor of an isolated island (Ref. 9). The form factor has been normalized by the particle volume. The numerical parameters have been given in Sec. II C.

ring of its interference fringes by the graded interface and the jump of index of refraction at the layer/substrate interface. However, for this peculiar case without any contrast between the layer and the substrate, the whole diffuse scattering [Eq. (2.14)] should vanish at $q_\parallel=0$ and the intensity should be concentrated in the specular beam [Eq. (2.12)].

2. Effect of the gradient of refraction index

The same conclusions can be drawn upon embedding a particle in different profiles of refraction index. Figure 4 illustrates such a behavior for a cylinder in various constant or parabolic profiles (see the inset of Fig. 4). The case of DWBA starting from the flat substrate surface[9] corresponds to the curve with $\delta_{\text{layer}}=0$ (downward triangles). The intensities calculated for the various profiles may vary by as much as 1 order of magnitude. Moreover, the fringes can be made sharper by modulating the profile, as shown in Fig. 4(b) for the parabolic profile (squares).

III. SCATTERING BY A DENSE SYSTEM OF CORRELATED PARTICLES

Because of the finite coherence length of the x-ray beam parallel to the surface and the finite detector angular acceptance, a measurement on a macroscopic scale S will be only sensitive to the configuration average $\langle \Phi(\mathbf{q}_\parallel, k_{iz}, k_{fz}) \rangle$ [Eq. (2.15)] over the coherently illuminated domains A_{coh}. This relies on an ergodicity hypothesis. Furthermore, the coherence domain A_{coh} is supposed to be large enough so that each subsurface of size A_{coh} in S presents the same statistical properties. For spatially homogeneous systems, this average can be decomposed into a coherent and an incoherent $\Phi_0(\mathbf{q}_\parallel, k_{iz}, k_{fz})$ diffuse scattering[10,32,40,41] as

$$\langle \Phi(\mathbf{q}_\parallel, k_{iz}, k_{fz}) \rangle = N \langle |\mathcal{F}(q_\parallel = 0, k_{iz}, k_{fz})|^2 \rangle \delta(q_\parallel) + \Phi_0(\mathbf{q}_\parallel, k_{iz}, k_{fz}) + \sum_{\beta,\alpha} p(\alpha) p(\beta) \times \mathcal{F}_\alpha(\mathbf{q}_\parallel, k_{iz}, k_{fz}) \mathcal{F}^*_\beta(\mathbf{q}_\parallel, k_{iz}, k_{fz}) S_{\alpha\beta}(\mathbf{q}_\parallel), \quad (3.1)$$

$$\Phi_0(\mathbf{q}_\parallel, k_{iz}, k_{fz}) = \langle |\mathcal{F}(\mathbf{q}_\parallel, k_{iz}, k_{fz})|^2 \rangle - |\langle \mathcal{F}(\mathbf{q}_\parallel, k_{iz}, k_{fz}) \rangle|^2, \quad (3.2)$$

$$S_{\alpha\beta}(\mathbf{q}_\parallel) = 1 + \rho_S \int_S [g_{\alpha\beta}(\mathbf{r}_\parallel) - 1] e^{i\mathbf{q}_\parallel \cdot \mathbf{r}_\parallel} d\mathbf{r}_\parallel, \quad (3.3)$$

where $p(\alpha)$ is the probability density of having a particle of kind α (which is defined by its shape and geometrical parameters) and of form factor $\mathcal{F}_\alpha(\mathbf{q}_\parallel, k_{iz}, k_{fz})$. The average over

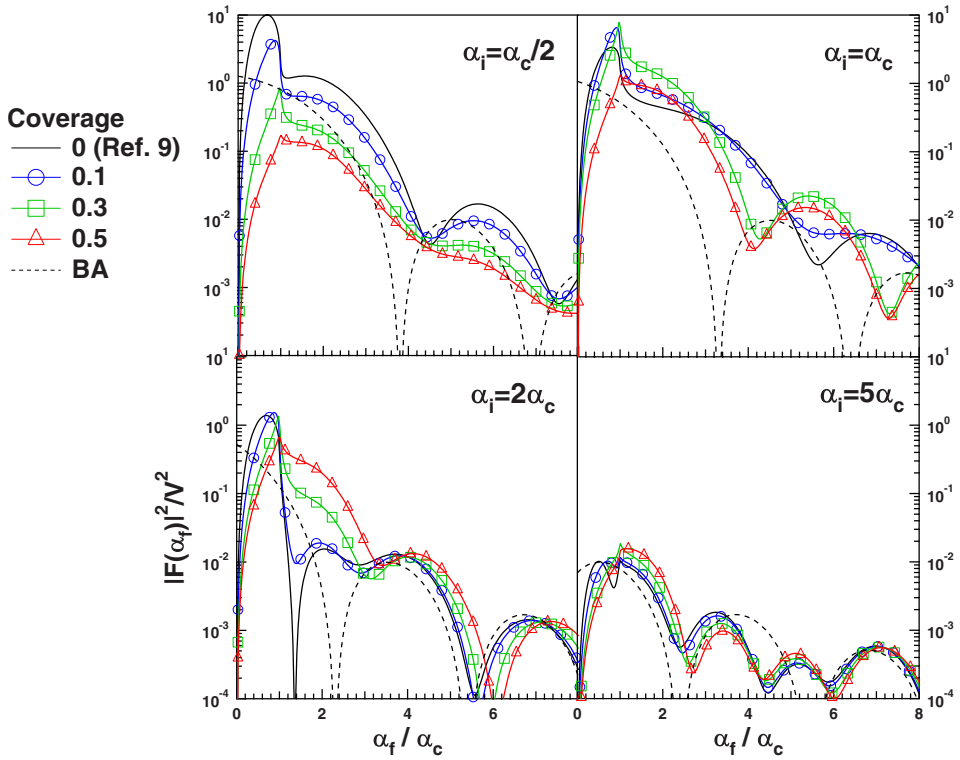

FIG. 3. (Color online) Same as Fig. 2 but the particle shape is a full sphere.

such a distribution is denoted by $\langle \cdots \rangle$. $S_{\alpha\beta}(\mathbf{q}_\parallel)$, known as the partial interference function, is the Fourier transform of the reduced partial particle pair correlation $g_{\alpha\beta}(\mathbf{r}_\parallel)$. ρ_S being the surface density of particles, $\rho_S p(\beta) g_{\alpha\beta}(\mathbf{r}_\parallel) d\mathbf{r}_\parallel$ is the number of particle of kind β at vector $\mathbf{r}_\parallel$ from a central particle of kind α. In the field of diffraction by crystals, the crystallographic counterpart of $\Phi_0(\mathbf{q}_\parallel, k_{iz}, k_{fz})$ is, for instance, the incoherent scattering cross section due to isotopic effects in neutron diffraction or the diffuse background due to the uncorrelated motions of atoms (known as the Debye-Waller or thermal diffuse scattering). In standard small-angle scattering, the second term of Eq. (3.1) is called "coherent" because it involves the interference phenomena between the waves scattered by various islands.

Even if the size and shape distributions of the islands can be reduced to a small number of parameters that allow us to compute the averages of Eq. (3.2), a practical use of Eq. (3.1) needs a deep knowledge of the microstructure of the system. Indeed, all the correlations between the size and shape of the scatterers are partially hidden in $S_{\alpha\beta}(\mathbf{q}_\parallel)$ [or $g_{\alpha\beta}(\mathbf{r}_\parallel)$]. Thus, approximations are used to overcome this problem.

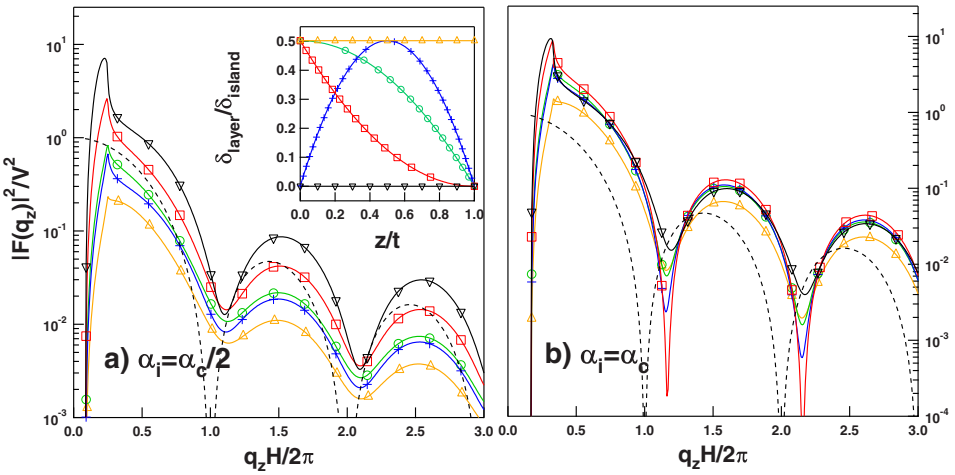

FIG. 4. (Color online) Modulus squared of a cylinder form factor at $\mathbf{q}_\parallel=0$ embedded in various gradients of refraction index for two incident angles: (a) $\alpha_i=\alpha_c/2$ and (b) $\alpha_i=\alpha_c$. The symbols correspond to the chosen gradients shown in the inset. The downward triangle symbol ($\delta_{layer}=0$) corresponds to the form factor of an isolated particle (Ref. 9). The cylinder height is equal to the layer thickness t. The Born term is also shown (dashed line). The form factor is normalized by the particle volume.

A. Classical approximations: Decoupling approximation and local monodisperse approximation

The first approximation, known as the decoupling approximation,[10,32,40–42] assumes that there is no correlation between the kinds of neighboring scatterers or between their kinds and relative positions; in other words, the partial interference (and thus the pair correlation functions) is independent of the particle kinds: $g_{\alpha\beta}(\mathbf{r}_\parallel)=g(\mathbf{r}_\parallel)$ and $S(\mathbf{q}_\parallel)=S_{\alpha\beta}(\mathbf{q}_\parallel)$. A factorization becomes possible into Eq. (3.1):

$$\langle\Phi(\mathbf{q}_\parallel,k_{iz},k_{fz})\rangle=\Phi_0(\mathbf{q}_\parallel)+|\langle\mathcal{F}(\mathbf{q}_\parallel,k_{iz},k_{fz})\rangle|^2S(\mathbf{q}_\parallel). \quad (3.4)$$

The DA relies on an hypothesis of full disorder, without any restriction on cluster overlapping.

The other approximation introduced by Pedersen[12] as the local monodisperse approximation[10–14] assumes that the scattering cross section results from an incoherent sum of scattering from monodisperse domains. This means that over the projected coherence length of the x-ray beam, the particles are all of the same size and shape. The scattered intensity thus appears as the average of the product of the particle form factor times the interference function inside each domain:

$$\langle\Phi(\mathbf{q}_\parallel,k_{iz},k_{fz})\rangle=\langle|\mathcal{F}(\mathbf{q}_\parallel,k_{iz},k_{fz})|^2S(\mathbf{q}_\parallel)\rangle. \quad (3.5)$$

A more restrictive formulation of this approximation (called hereafter LMA 0) is obtained by assuming the same spatial organization [and thus $S(\mathbf{q}_\parallel)$] in each domain:

$$\langle\Phi(\mathbf{q}_\parallel,k_{iz},k_{fz})\rangle=\langle|\mathcal{F}(\mathbf{q}_\parallel,k_{iz},k_{fz})|^2\rangle S(\mathbf{q}_\parallel). \quad (3.6)$$

Although very appealing in terms of data analysis, the LMA relies on an unphysical description of the microstructure for most of the studied experimental systems.

For disordered systems, the DA and the LMA lead to the same results at high wave vector transfer where the scattering is sensitive only to the average particle form factor. However, measurements in such a high $q_\parallel$ limit are often hampered by the decrease of intensity and the residual background. Furthermore, precious information, among others the particle density, is available around and below the maximum of scattered intensity, the so-called correlation peak. In this $q_\parallel$ range, a too intense scattering due to the incoherent term[15] [Eq. (3.2)] shows up in the DA, a drawback that seems to be cured in the LMA. This explains that most data analyses are performed within the LMA.[12,15,38,43,53] Recent experimental results based on combined GISAXS and transmission electron microscopy (TEM) measurements[15] have evidenced, for a nucleation-growth-coalescence scenario of metal islands on oxide support, the scattering signature of spatial correlations between islands. As shown by TEM, the sizes of nearest neighboring islands are not correlated to the central particle size. However, the larger the central particle size, the farther its nearest neighbors. This hard-core-type effect results from a scaling of the Voronoï cell with the particle lateral size[54–56] and induces a strong decrease of intensity below the correlation peak. Leroy *et al.*[45] have introduced a one dimensional model in the framework of the paracrystal[41,46–48] to account for such correlations. Such models have been applied to the scattering from terraces on surfaces.[57–59] The following section is intended to generalize such a model to 3D particles along a chain and to compare it with the DA and the LMA.

B. Scattering by a one dimensional chain of correlated particles

1. General formalism of the size-spacing coupling approximation

The formalism of this section is restricted to the Born approximation (i.e., simple Fourier transform) but it is straightforwardly generalized to the previously developed DWBA upon introducing the appropriate form factor, as the parallel and z directions behave independently in the calculation of $\mathcal{F}(\mathbf{q}_\parallel,k_{iz},k_{fz})$. Let us call $r_\parallel$ (or x) the direction along the chain, whereas the $\mathbf{r}_\perp$ or $\mathbf{z}$ (y and z) directions are perpendicular to the particle alignment (see Fig. 1). The autocorrelation function $Z_+(r_\parallel,\mathbf{r}_\perp)$ for $r_\parallel\geqslant 0$ is calculated step by step along the chain from the knowledge of (i) the joint density probability $p(\alpha_0,\ldots,\alpha_n)$ of having a $\alpha_0,\ldots,\alpha_n$ sequence of particles of kind α_i along the chain and (ii) the conditional density probability of having an algebraic distance d_n between the particles $n-1$ and n, knowing the sequence $\alpha_0,\ldots,\alpha_n$ i.e., $P_n(d_n/[\alpha_0,\ldots,\alpha_n])$:

$$Z_+(r_\parallel,\mathbf{r}_\perp)=z_0(r_\parallel,\mathbf{r}_\perp)+z_+(r_\parallel,\mathbf{r}_\perp), \quad (3.7)$$

$$z_0(r_\parallel,\mathbf{r}_\perp)=\int p(\alpha_0)\{\mathcal{S}_0(-x,-\mathbf{z},\alpha_0)\otimes\mathcal{S}_0(x,\mathbf{z},\alpha_0)\otimes\delta(x)\}(r_\parallel,\mathbf{r}_\perp)d\alpha_0, \quad (3.8)$$

$$\begin{aligned}z_+(r_\parallel,\mathbf{r}_\perp)=&\int\int p(\alpha_0,\alpha_1)\{\mathcal{S}_0(-x,-\mathbf{z},\alpha_0)\otimes\mathcal{S}_1(x,\mathbf{z},\alpha_1)\\&\otimes P_1(x/[\alpha_0,\alpha_1])\}(r_\parallel,\mathbf{r}_\perp)d\alpha_0d\alpha_1\\&+\int\int\int p(\alpha_0,\alpha_1,\alpha_2)\{\mathcal{S}_0(-x,-\mathbf{z},\alpha_0)\\&\otimes\mathcal{S}_2(x,\mathbf{z},\alpha_2)\otimes P_1(x/[\alpha_0,\alpha_1])\\&\otimes P_2(x/[\alpha_0,\alpha_1,\alpha_2])\}(r_\parallel,\mathbf{r}_\perp)d\alpha_0d\alpha_1d\alpha_2+\cdots.\end{aligned} \quad (3.9)$$

$\otimes$ is the convolution product in space and, as previously, $\mathcal{S}(x,\mathbf{z},\alpha)$ is the shape function of the particle of kind α. Indeed, the probability of having a given distance d between the origin and the nth particle is the integral of the product of all the probabilities of the intermediate distances between particles before the nth; the constraint that the sum of such distances is d shows that the required probability is the folding product of all the intermediate distance probabilities. After having introduced $\mathcal{P}_n(q_\parallel/[\alpha_0,\ldots,\alpha_n])$ as the Fourier transform along the chain of $P(d_n/[\alpha_0,\ldots,\alpha_n])$, the BA scattered intensity per particle is obtained by simple Fourier transform of the total autocorrelation function $Z(r_\parallel,\mathbf{r}_\perp)=z_0(r_\parallel,\mathbf{r}_\perp)+z_+(r_\parallel,\mathbf{r}_\perp)+z_-(r_\parallel,\mathbf{r}_\perp)$, with $z_-(r_\parallel,\mathbf{r}_\perp)=z_+(-r_\parallel,-\mathbf{r}_\perp)$:

$$\langle \Phi(q_\parallel, \mathbf{q}_\perp) \rangle = \tilde{z}_0(\mathbf{q}_\perp)\delta(q_\parallel) + \int p(\alpha_0)|\mathcal{F}_0(\alpha_0, q_\parallel, \mathbf{q}_\perp)|^2 d\alpha_0 + 2\,\mathrm{Re}\left\{ \int\int p(\alpha_0,\alpha_1)\mathcal{F}_0^*(q_\parallel,\mathbf{q}_\perp,\alpha_0)\mathcal{F}_1(q_\parallel,\mathbf{q}_\perp,\alpha_1)\mathcal{P}_1(q_\parallel/[\alpha_0,\alpha_1])d\alpha_0 d\alpha_1 + \int\int\int p(\alpha_0,\alpha_1,\alpha_2)\mathcal{F}_0^*(q_\parallel,\mathbf{q}_\perp,\alpha_0)\mathcal{F}_2(q_\parallel,\mathbf{q}_\perp,\alpha_2)\mathcal{P}_1(q_\parallel/[\alpha_0,\alpha_1])\mathcal{P}_2(q_\parallel/[\alpha_0,\alpha_1,\alpha_2])d\alpha_0 d\alpha_1 d\alpha_2 + \cdots \right\}. \tag{3.10}$$

A divergence proportional to the size of the system appears at the origin ($q_\parallel \to 0$) where all the particles scatter exactly in phase. It is proportional to $V(\alpha, \mathbf{q}_\perp)$, the $q_\parallel = 0$ limit of the form factor which reduces to the volume of the particle at $\mathbf{q}_\perp = 0$. For convenience, the term "volume" will be used hereafter for this limit.

To go further on, a complete lack of correlation between the sizes of neighboring particles will be assumed, $p(\alpha_0, \ldots, \alpha_n) = p(\alpha_0)\ldots p(\alpha_n)$, but, to account for an exclusion volume effect, the distance between two neighbors is supposed to depend linearly on their respective sizes $R_\parallel(\alpha_i)$ along the chain direction. This size-spacing correlation approximation (SSCA) is included into $P_n(d_n/[\alpha_0, \ldots, \alpha_n])$ through

$$\int_{-\infty}^{+\infty} d_n P_n(d_n/[\alpha_0, \ldots, \alpha_n])dd_n = D + \kappa[\Delta R_\parallel(\alpha_{n-1}) + \Delta R_\parallel(\alpha_n)], \tag{3.11}$$

with $\Delta R_\parallel(\alpha_i) = R_\parallel(\alpha_i) - \langle R_\parallel(\alpha) \rangle$. D and $\langle R_\parallel(\alpha) \rangle$ are, respectively, the average distance along the chain between particles irrespective of their sizes and the parallel average radius. This gives in reciprocal space

$$\mathcal{P}_n(q_\parallel/[\alpha_0, \ldots, \alpha_n]) = \phi(q_\parallel) e^{iq_\parallel D} e^{i\kappa q_\parallel [\Delta R_\parallel(\alpha_{n-1}) + \Delta R_\parallel(\alpha_n)]}, \tag{3.12}$$

where κ is the size-spacing coupling parameter. $\kappa > 0$ corresponds to an increase of the average distance between nearest neighbors as function of their sizes. It is worth noticing that in the $\kappa = 0$ limit, Eq. (3.12) gives the statistic of the classical paracrystal in reciprocal space $\phi(q_\parallel)e^{iq_\parallel D}$.[41] The introduction of these two approximations in Eq. (3.10) yields

$$\langle \Phi(q_\parallel), \mathbf{q}_\perp \rangle = \tilde{z}_0(\mathbf{q}_\perp)\delta(q_\parallel) + |\langle \mathcal{F}(q_\parallel, \mathbf{q}_\perp) \rangle|^2 + 2\,\mathrm{Re}\left\{ \sum_{n=1}^{+\infty} \Gamma_n(q_\parallel, \mathbf{q}_\perp) \right\},$$

$$\Gamma_n(q_\parallel, \mathbf{q}_\perp) = \phi^n(q_\parallel)\exp(inq_\parallel D) \int \cdots \int p(\alpha_0)\cdots p(\alpha_n)\mathcal{F}^*(q_\parallel, \mathbf{q}_\perp, \alpha_0)\mathcal{F}(q_\parallel, \mathbf{q}_\perp, \alpha_n) \times \exp\left\{ i\kappa q_\parallel \left[\Delta R_\parallel(\alpha_0) + 2\sum_{k=1}^{n-1} \Delta R_\parallel(\alpha_k) + \Delta R_\parallel(\alpha_n) \right] \right\} d\alpha_0 \cdots d\alpha_n. \tag{3.13}$$

This writing along a geometric series allows us to carry out the summation in Eq. (3.13):

$$\langle \Phi(q_\parallel, \mathbf{q}_\perp) \rangle = \tilde{z}_0(\mathbf{q}_\perp)\delta(q_\parallel) + |\langle \mathcal{F}(q_\parallel, \mathbf{q}_\perp) \rangle|^2 + 2\,\mathrm{Re}\left\{ \tilde{\mathcal{F}}_\kappa(q_\parallel, \mathbf{q}_\perp)\widetilde{\mathcal{F}^*}_\kappa(q_\parallel, \mathbf{q}_\perp) \frac{\Omega_\kappa(q_\parallel)}{\tilde{p}_{2\kappa}(q_\parallel)[1 - \Omega_\kappa(q_\parallel)]} \right\}, \tag{3.14}$$

$$\Omega_\kappa(q_\parallel) = \tilde{p}_{2\kappa}(q_\parallel)\phi(q_\parallel)e^{iq_\parallel D}. \tag{3.15}$$

The characteristic function of the particle kind distribution evaluated along the parallel size distribution was introduced in the previous equation:

$$\tilde{p}_\kappa(q_\parallel) = \int p(\alpha) e^{i\kappa q_\parallel \Delta R_\parallel(\alpha)} d\alpha. \tag{3.16}$$

$\tilde{\mathcal{F}}_\kappa(\mathbf{q}_\parallel)$ is defined as

$$\tilde{\mathcal{F}}_\kappa(q_\parallel, \mathbf{q}_\perp) = \int p(\alpha)\mathcal{F}(q_\parallel, \mathbf{q}_\perp, \alpha) e^{i\kappa q_\parallel \Delta R_\parallel(\alpha)} d\alpha. \tag{3.17}$$

It is a generalization of the particle form factor averaged over

the size-shape distribution. Notice that in Eq. (3.14) the complex conjugate is applied to the particle form factor before the averaging over α [Eq. (3.17)].

The total interference function $S(q_\parallel)$ follows from Eq. (3.14) upon replacement of the particle shape by a Dirac peak i.e., the particle form factor $\mathcal{F}(q_\parallel,\mathbf{q}_\perp,\alpha)$, by 1:

$$S(q_\parallel) = 1 + 2\,\mathrm{Re}\left\{\frac{\tilde{p}_\kappa^2(q_\parallel)\Omega_\kappa(q_\parallel)}{\tilde{p}_{2\kappa}(q_\parallel)[1-\Omega_\kappa(q_\parallel)]}\right\}. \tag{3.18}$$

If $\kappa=0$, $\tilde{\mathcal{F}}_\kappa(q_\parallel,\mathbf{q}_\perp)=\langle\mathcal{F}(q_\parallel,\mathbf{q}_\perp,\alpha)\rangle$ and $\tilde{p}_{2\kappa}(q_\parallel)=1$. Thus, Eq. (3.14) reduces to the DA with an interference function given by the Hosemann 1D paracrystal:[41]

$$\langle\Phi(q_\parallel,\mathbf{q}_\perp)\rangle = \tilde{z}_0(\mathbf{q}_\perp)\delta(q_\parallel) + \langle|\mathcal{F}(q_\parallel,\mathbf{q}_\perp,\alpha)|^2\rangle - |\langle\mathcal{F}(q_\parallel,\mathbf{q}_\perp)\rangle|^2 + |\langle\mathcal{F}(q_\parallel,\mathbf{q}_\perp,\alpha)\rangle|^2 S_p(q_\parallel),$$

$$S_p(q_\parallel) = \frac{1-\phi^2(q_\parallel)}{1+\phi^2(q_\parallel)-2\phi(q_\parallel)\cos(q_\parallel D)}. \tag{3.19}$$

2. Behavior at ($q_\parallel=0$, $\mathbf{q}_\perp\neq\mathbf{0}$)

The details of the calculation at $q_\parallel=0$ of Eq. (3.14) are given in Appendix A as function of the particle volume $V(\alpha,\mathbf{q}_\perp)$:

$$\langle\Phi(q_\parallel,\mathbf{q}_\perp)\rangle \simeq \langle V(\alpha,\mathbf{q}_\perp)^2\rangle - \langle V(\alpha,\mathbf{q}_\perp)\rangle^2 + \frac{\sigma_D^2+4\kappa^2\sigma_{R_\parallel}^2}{D^2}\langle V(\alpha,\mathbf{q}_\perp)\rangle^2 - \frac{4\kappa}{D}\langle V(\alpha,\mathbf{q}_\perp)\rangle\langle V(\alpha,\mathbf{q}_\perp)\Delta R_\parallel(\alpha)\rangle, \tag{3.20}$$

where σ_D and $\sigma_{R_\parallel}$ are the second moment of the distance distribution $P(d_n)$ of the paracrystal and of the size-shape distribution $p(\alpha)$, respectively. Of course, the singular term $\tilde{z}_0(\mathbf{q}_\perp)\delta(q_\parallel,\mathbf{q}_\perp)$ is excluded on purpose. As shown in Refs. 10, 40, and 41, this limit is related to the fluctuations of the electronic density in the probed volume. However, a coupling term $\frac{4\kappa}{D}\langle V(\alpha,\mathbf{q}_\perp)\rangle\langle V(\alpha,\mathbf{q}_\perp)\Delta R_\parallel(\alpha)\rangle$ reduces the simple variance sum of either (i) the particle size-shape distributions ($\langle V(\alpha,\mathbf{q}_\perp)^2\rangle-\langle V(\alpha,\mathbf{q}_\perp)\rangle^2$), (ii) the intrinsic paracrystalline disorders $\frac{\sigma_D^2}{D^2}\langle V(\alpha,\mathbf{q}_\perp)\rangle^2$, or (iii) that due to the parallel size distribution $\frac{4\kappa^2\sigma_{R_\parallel}^2}{D^2}\langle V(\alpha,\mathbf{q}_\perp)\rangle^2$). This leads to a minimum of the $q_\parallel=0$ scattered intensity as function of κ at

$$\kappa_0(\mathbf{q}_\perp) = \frac{1}{2}\frac{D}{\sigma_{R_\parallel}^2}\frac{\langle V(\alpha,\mathbf{q}_\perp)\Delta R_\parallel(\alpha)\rangle}{\langle V(\alpha,\mathbf{q}_\perp)\rangle} \tag{3.21}$$

as $\partial^2\langle\Phi(q_\parallel)\rangle/\partial\kappa^2 = 8\sigma_{R_\parallel}^2\langle V(\alpha,\mathbf{q}_\perp)\rangle^2/D^2 > 0$. Of course, this conclusion applies if the singular term of Eq. (3.10) is excluded.

For a 1D particle with $V\propto R_\parallel$, $\kappa_0(\mathbf{q}_\perp)=D/2\langle R_\parallel(\alpha)\rangle$. For a particle of higher dimensionality, $\kappa_0(\mathbf{q}_\perp)$ depends on the degree of correlation between the parallel direction and the other ones in the volume expression. However, for $V\propto R_\parallel^n$, to first order in $\sigma_{R_\parallel}/\langle R_\parallel(\alpha)\rangle$, $\kappa_0\simeq nD/2\langle R_\parallel(\alpha)\rangle$.

3. Finite-size effects

In line with the works about the paracrystal model,[12,41,48,60–62] scattering by a finite-size chain made of N particles can be accounted for by folding Eq. (3.9) with the chain shape function. In reciprocal space, the consequence is a restriction of the summation in Eq. (3.13) to the number of particles N:

$$\langle\Phi(q_\parallel,\mathbf{q}_\perp)\rangle = |\langle\mathcal{F}(q_\parallel,\mathbf{q}_\perp)\rangle|^2 + \frac{2}{N}\,\mathrm{Re}\left\{\sum_{n=1}^{N-1}(N-n)\Gamma_n(q_\parallel,\mathbf{q}_\perp)\right\}, \tag{3.22}$$

where $N-n$ is the number of lattice points common to the chain and its folding counterpart shifted by n cells. The geometric sum series in Eqs. (3.12), (3.13), and (3.22) leads to

$$\langle\Phi(q_\parallel,\mathbf{q}_\perp)\rangle = |\langle\mathcal{F}(q_\parallel,\mathbf{q}_\perp)\rangle|^2 + 2\,\mathrm{Re}\left\{\frac{1}{\tilde{p}_{2\kappa}(q_\parallel)}\tilde{\mathcal{F}}_\kappa(q_\parallel,\mathbf{q}_\perp)\widetilde{\mathcal{F}^*}_\kappa(q_\parallel,\mathbf{q}_\perp) \times\left[\left(1-\frac{1}{N}\right)\frac{\Omega_\kappa(q_\parallel)}{1-\Omega_\kappa(q_\parallel)} - \frac{2}{N}\frac{\Omega_\kappa(q_\parallel)^2[1-\Omega_\kappa(q_\parallel)^{N-1}]}{[1-\Omega_\kappa(q_\parallel)]^2}\right]\right\}. \tag{3.23}$$

Equation (3.23) includes in a continuous way the ($q_\parallel=0,\mathbf{q}_\perp$) line; the Dirac peak $\tilde{z}_0(\mathbf{q}_\perp)\delta(q_\parallel)$ is broadened with a width inversely proportional to the size of the chain. It is usual to account for a broad distribution of chain lengths by replacing the $1-n/N$ term in Eq. (3.23) with an exponential cut-off function $e^{-nD/\Lambda}$ which allows us to extend the summation to infinity. Λ is interpreted as the coherence length of the chain. This empirical method[58] is a way to account for the experimentally observed Lorentzian shape of the central peak. In this case, Eq. (3.14) should be modified by replacing $\Omega_\kappa(q_\parallel)$ by $\Omega_{fs}(q_\parallel)=\tilde{p}_{2\kappa}(q_\parallel,\mathbf{q}_\perp)\phi(q_\parallel)e^{iq_\parallel D}e^{-D/\Lambda}$ and $\tilde{z}_0(\mathbf{q}_\perp)\delta(q_\parallel)$ dropped. In this way, using the DWBA for a graded interface, the specular rod term is included in the formula but with a broadening that does not account for the instrumental resolution (i.e., the wavelength and incident angle distributions, the angular resolution of the detector, etc.).

4. Examples and comparison between decoupling approximation, local monodisperse approximation 0, local monodisperse approximation, and size spacing correlation approximation

The DA, LMA 0, and 1D SSCA are compared in Figs. 5 and 6 for a cylindrical particle and for a typical GISAXS experiment, including the specular rod through a correlation length of $\Lambda=100D$ in Fig. 6. The size distribution as well as the paracrystal spacing probability have been taken as Gaussian:

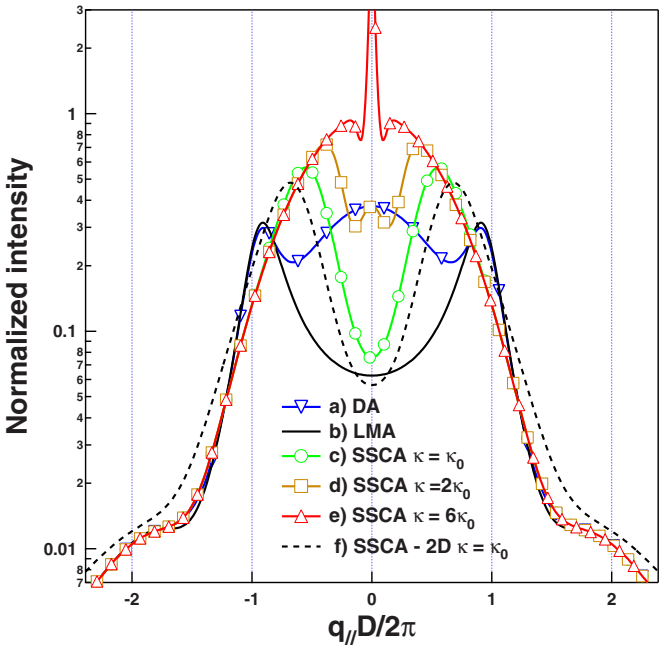

FIG. 5. (Color online) Scattering $\langle \Phi(q_\parallel, q_\perp = 0) \rangle$ from a 1D infinite chain of cylinders within various frameworks (DA, LMA 0, SSCA). For the SSCA, $\kappa = \kappa_0(\mathbf{q}_\perp = 0)$ is the special value of the coupling parameter for which the intensity is minimum at $q_\parallel = 0$. The intensity is normalized by $\langle V^2(\alpha) \rangle$. Both the size and chain statistics are Gaussian with $\sigma_{R_\parallel}/\langle R_\parallel \rangle = 0.25$, $\sigma_D/D = 0.25$, and $D = 3\langle R_\parallel \rangle$. The particle aspect ratio $H/R = 1$ is fixed, i.e., the particle volume V scales with $R_\parallel^3$; for the case "2D" where $H/\langle R_\parallel \rangle = 1$, $V \sim R_\parallel^2$.

$$p(\Delta R_\parallel) = \frac{1}{\sigma_{R_\parallel}\sqrt{2\pi}} \exp\left\{ -\frac{\Delta R_\parallel^2}{2\sigma_{R_\parallel}^2} \right\},$$

$$P_n(d_n/[R_\parallel(\alpha_{n-1}), R_\parallel(\alpha_n)]) = \frac{1}{\sigma_D\sqrt{2\pi}} \exp\left\{ -\frac{[d_n - D - \kappa(\Delta R_\parallel(\alpha_{n-1}) + \Delta R_\parallel(\alpha_n))]^2}{2\sigma_D^2} \right\}. \quad (3.24)$$

The first important point is that all the used approximations (DA, LMA 0, SSCA) are equivalent at large parallel wave vector transfer $q_\parallel$; "large" means well above the correlation peak, i.e., the maximum of scattering. In this regime, the loss of long range order results in a scattering pattern which is only sensitive to the particle form factor. The differences between the various approximations (independent of their physical relevance) show up at and below the correlation peak. As already highlighted in Refs. 15, 16, and 45, the intense scattering found at small parallel wave vector transfer (or small in-plane scattering angle $2\theta_f$) in the DA [see Fig. 5 and 6(a)] is cured in the LMA 0 [see Fig. 5(b) and 6(b)] with a maximum of intensity slightly shifted from the first peak of the paracrystal interference function $S_p(q_\parallel)$ [Eq. (3.19)] because of the local slope of the form factor.[16] The introduction of partial correlation between the neighboring particle sizes and their distance yields strong modification of the scattering

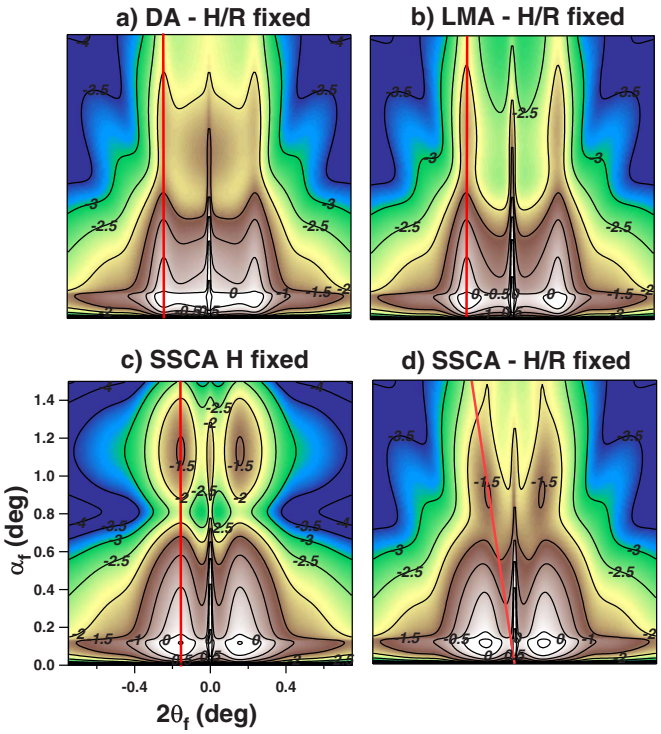

FIG. 6. (Color online) Small-angle scattering under grazing incidence $\langle \Phi(2\theta_f, \alpha_f) \rangle$ from a polydispersed chain of cylinders. The calculations are performed within the simple DWBA with the parameters of Sec. II C. The size distribution as well as the intrinsic paracrystal statistics are Gaussian with $\sigma_{R_\parallel}/\langle R_\parallel \rangle = 0.25$ and $\sigma_D/D = 0.25$. The chain correlation length is $\Lambda = 100D$ with $D = 3\langle R_\parallel \rangle$. The intensity normalized by the mean squared volume $\langle V(\alpha)^2 \rangle$ is displayed on a logarithmic scale given by the isolines. The particle aspect ratio is constant $H/R = 1$, except for case (c) where the particle height is kept constant at $H/\langle R_\parallel \rangle = 1$. The following frameworks are used: (a) decoupling approximation [Eq. (3.4)], (b) local monodispersed approximation without correlations LMA 0 [Eq. (3.6)], and [(c) and (d)] size-spacing coupling approximation at $\kappa = \kappa_0(\mathbf{q}_\perp = 0)$ [Eq. (3.21)]. The red lines are guides for the eyes to highlight the correlation induced tilt of second order scattering lobes in $q_\perp$.

curve shape. In particular, the position of the maximum of intensity [Figs. 5(a) and 5(c)–5(e)] is no more simply related to the mean particle separation D as expected in the DA or LMA 0 approximation where the partial interference functions are reduced to a common function. Instead, in the SSCA, the correlation peak position decreases upon an increase of the coupling parameter κ. At $\kappa = \kappa_0(\mathbf{q}_\perp = 0)$, a minimum of intensity equivalent to that of the LMA 0 is also found, whereas at higher κ values, the correlation peak merges with the specular rod. The observed broadness of the correlation peak in the SSCA (as compared to the width of a simple paracrystal interference function [Eq. (3.19)]) is linked to the different partial interference functions; the associated partial pair correlation functions yield a distribution of preferential distances that reproduces in some way the particle size distribution.[45] The $\kappa_0(\mathbf{q}_\perp)$ value and the associated scattering curve depend on the dimensionality of the particle. Indeed, the results for a particle with fixed aspect

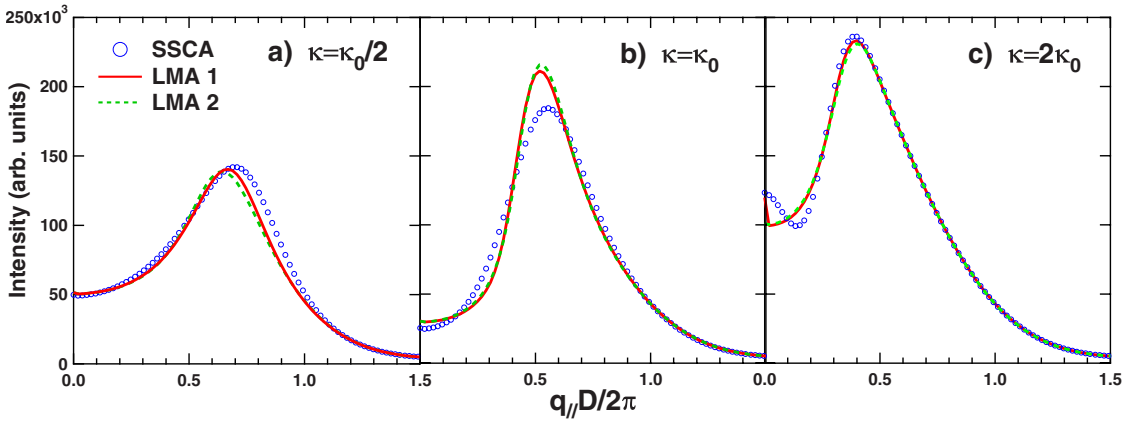

FIG. 7. (Color online) Best fit of the SSCA scattering curves (points) using LMA [Eq. (3.5)] with correlations between size $R_\parallel$ and spacing d_n in each domain: $d_n=D+2\kappa\Delta R_\parallel$ (LMA 1) or $d_n=2\kappa R_\parallel$ (LMA 2). The numerical parameters for the SSCA curves are identical to those of Fig. 5 except the value of κ. The fitted parameters are given in Table I.

ratio $H/R_\parallel$ are completely different from those obtained at fixed height [see Figs. 5(c), 5(f), 6(c), and 6(d)]: the scattering weight of the particle scales with $R_\parallel^3$ in the first case and $R_\parallel^2$ in the second. An amazing signature is found in the GISAXS maps. In the DA, LMA 0, or SSCA at fixed height, the scattering lobes along $q_\perp$ or α_f due to the mean particle height have axes oriented along the $(q_\parallel, q_\perp)$ directions following exactly the behavior of the Kiessig fringes even along the specular direction. In SSCA at fixed aspect ratio, the lobe principal axis is tilted and points toward the origin of the reciprocal space [see the line on Fig. 6(d)]. Indeed, the biggest particles, which perpendicular scattering lobes are closer, are also farthest apart and thus scatter at the smallest parallel wave vector transfer. The inverse applies for the smaller ones. Notice that the α_f locations of the lobes are quite different in SSCA at fixed height or fixed aspect ratio, i.e., fluctuating height. Moreover, the interference fringes on top of the correlation peak are no more inevitably in phase with the specular Kiessig fringes after correction of the Ewald sphere curvature. The link between the tilt angle and the correlation coefficient is indirect and depends on the cross correlation between the parallel and perpendicular dimensions of the particles. These inclined lobes should not be misinterpreted as an effect of scattering from faceted particles.[5,15]

The effect of correlations can be introduced also in the LMA by assuming that the interference function of each monodisperse domain depends on the size of the particles[12] [Eq. (3.5)]. To assess if LMA with correlations is able to reproduce SSCA effects in one dimension, it has been chosen to fit the SSCA scattering curves with the LMA model while keeping the same framework of Gaussian paracrystal and size distribution [Eq. (3.24)]. Two dependences for the mean distance in each domain have been chosen: $d_n=D+2\kappa\Delta R_\parallel$ (LMA 1) as introduced in the SSCA or $D=2\kappa R_\parallel=2\kappa\langle R_\parallel\rangle+2\kappa\Delta R_\parallel$ (LMA 2). Good fits can be obtained as shown in Fig. 7 for various values of κ(SSCA); the fitted parameters are gathered in Table I. If fitted (not shown), the mean radius $\langle\sigma_{R_\parallel}\rangle$ and the width of the size distribution $\sigma_\parallel$ agree to within less than a few percents with the chosen ones. As already stated, these parameters are mainly imposed by the high-$q_\parallel$ range. As compared to SSCA, the mean distance D and the paracrystal disorder are overestimated by $\sim$10%–35% and 80%–250%, respectively, while the size-distance coupling parameter κ is underestimated by 40%–80%. Similar trends (not shown) have been observed upon varying $\sigma_{R_\parallel}$ and σ_D. Interestingly, the variance of the particle spacing $\sigma_{d_n}^2=\langle(d_n-D)^2\rangle$ [$\sigma_{d_n}^2$(SSCA)$=\sigma_D^2+2\kappa^2\sigma_{R_\parallel}^2$ or $\sigma_{d_n}^2$(LMA)$=\sigma_D^2+4\kappa^2\sigma_{R_\parallel}^2$; see Appendix B] seems to be kept constant during the fit, while the relative weights of the components of spacing disorder are differently treated in SSCA and LMA; as compared to SSCA, LMA overestimates the standard paracrystalline disorder σ_D^2 and underestimates the contribution of the size

TABLE I. Parameters corresponding to the fit of the SSCA scattering curves with LMA (see Fig. 7): mean distance D, paracrystal disorder σ_D, size-spacing coupling parameter κ, and standard deviation of the spacing σ_{d_n} (see Appendix B). $D_0=D$(SSCA) and $\kappa_0=\kappa_0$(SSCA) are used to normalized the values. If fitted, $\langle R_\parallel\rangle$ and $\sigma_{R_\parallel}$ are equal to within less than 2% to the SSCA value, i.e., $\sigma_{R_\parallel}/\langle R_\parallel\rangle$(SSCA)$=0.25$.

	Fig. 7(a)				Fig. 7(b)				Fig. 7(c)			
	D/D_0	σ_D/D_0	κ/κ_0	σ_{d_n}/D_0	D/D_0	σ_D/D_0	κ/κ_0	σ_{d_n}/D_0	D/D_0	σ_D/D_0	κ/κ_0	σ_{d_n}/D_0
SSCA	1	0.25	0.5	0.34	1	0.25	1	0.54	1	0.25	2	0.98
LMA 1	1.13	0.46	0.06	0.46	1.16	0.47	0.61	0.6	1.28	0.91	0.65	1.1
LMA 2	1.09	0.44	0.49	0.35	1.26	0.49	0.5	0.58	1.36	0.93	0.5	0.98

fluctuations $\kappa^2\sigma_{R_\parallel}^2$ but reproduces more or less accurately $\sigma_{d_n}^2$.

IV. CONCLUSIONS

A different method for the analysis of GISAXS patterns from islands on surfaces has been proposed. Firstly, the DWBA perturbation formalism used for grazing incidence and emergence was applied to the graded interface, accounting for the propagation effects inside the island layer. It was demonstrated that the effective scattering form factor depends on the particle coverage and on the average profile of refraction index. Secondly, the introduced correlation between the size and the spacing between particles (SSCA) leads to a strong interplay between coherent and incoherent scattering in the direction parallel to the substrate. A special value of the coupling parameter gives rise to a minimum of scattered intensity at $q_\parallel=0$ as experimentally observed. The SSCA is more suitable than the classical DA or LMA in terms of introduced hypothesis on the morphology. A weakness of the SSCA is its 1D character; however, a generalization to two dimensions is foreseen in the framework of the ideal two-dimensional (2D) paracrystal[41,63] as well as the introduction of higher order correlations (as, for instance, between the sizes of particles). In a companion paper (Ref. 1), the herein developed models are successfully applied to the GISAXS study of the growth mode of Au nanoparticles on $TiO_2(110)$.

ACKNOWLEDGMENT

R.L. would like to acknowledge fruitful discussions with Fabio Finocchi (INSP-Paris) on the scattering theory.

APPENDIX A: SMALL WAVE VECTOR LIMIT IN THE ONE-DIMENSIONAL SIZE-SPACING CORRELATION APPROXIMATION

An expansion of the Fourier transform (i.e., characteristic functions) of the size-shape [Eq. (3.16)] and intrinsic paracrystal statistics $\phi(q_\parallel)$ up to second order in $q_\parallel$ gives

$$\tilde{p}_{2\kappa}(q_\parallel) \simeq 1 - 2\kappa^2 q_\parallel^2 \sigma_{R_\parallel}^2,$$

$$\phi(q_\parallel)e^{iq_\parallel D} \simeq 1 + iq_\parallel D - \frac{1}{2}q_\parallel^2(D^2+\sigma_D^2). \tag{A1}$$

The previous expansion assumes that the second order moment of the size-shape and of the paracrystal statistics, $\sigma_{R_\parallel}$ and σ_D, respectively, do exist, i.e., that the associated distributions are not pathological. This leads to zero order in $q_\parallel$ to

$$\frac{\phi(q_\parallel)e^{iq_\parallel D}}{1-\tilde{p}_{2\kappa}(q_\parallel)\phi(q_\parallel)e^{iq_\parallel D}} \simeq \frac{i}{q_\parallel D} - \frac{1}{2}\left(1 - \frac{\sigma_D^2 + 4\kappa^2\sigma_{R_\parallel}^2}{D^2}\right). \tag{A2}$$

To obtain the small wave vector limit of Eq. (3.14), it is thus necessary to expand the generalized particle form factor $\tilde{\mathcal{F}}_\kappa(\mathbf{q}_\parallel,\mathbf{q}_\perp)$ [Eq. (3.17)] and the mean form factor $\langle|\mathcal{F}(q_\parallel,\mathbf{q}_\perp,\alpha)|^2\rangle$ to first and zero order, respectively:

$$\langle|\mathcal{F}(q_\parallel,\mathbf{q}_\perp,\alpha)|^2\rangle \simeq \langle V(\alpha,\mathbf{q}_\perp)^2\rangle,$$

$$\tilde{\mathcal{F}}_\kappa(\mathbf{q}_\parallel,\mathbf{q}_\perp)\widetilde{\mathcal{F}^*}_\kappa(\mathbf{q}_\parallel,\mathbf{q}_\perp) \simeq \langle V(\alpha,\mathbf{q}_\perp)\rangle^2 + i\kappa q_\parallel\langle V(\alpha,\mathbf{q}_\perp)\Delta R_\parallel(\alpha)\rangle \times\langle V(\alpha,\mathbf{q}_\perp)\rangle. \tag{A3}$$

$V(\alpha,\mathbf{q}_\perp)$ is the value of the form factor of a particle of kind α at $q_\parallel=0$; it amounts to the volume of the particle at $\mathbf{q}_\perp=0$. Of course, Eqs. (A3) assume that the mean values over the size and shape distributions including $V(\alpha,\mathbf{q}_\perp)$ do exist, i.e., that the moments of order greater than 2 (depending on the particle dimensionality) are available. By introducing Eqs. (A2) and (A3), the limit at the origin, $q_\parallel=0$, of the scattered intensity [Eq. (3.14)] is given by Eq. (3.20). It is straightforward to show that this limit corresponds to an extremum, i.e., that the next term in the expansion is of second order.

APPENDIX B: VARIANCE OF THE PARTICLE SPACING

In SSCA, the variance of the spacing between particles is given by

$$\begin{aligned}\sigma_{d_n}^2(\mathrm{SSCA}) &= \langle(d_n - D)^2\rangle \\ &= \int\int p[\Delta R_\parallel(\alpha_{n-1})]p[\Delta R_\parallel(\alpha_n)]d\Delta R_\parallel(\alpha_{n-1}) \\ &\quad\times d\Delta R_\parallel(\alpha_n)\int dd_n(d_n-D)^2 \\ &\quad\times P_n(d_n/[R_\parallel(\alpha_{n-1}),R_\parallel(\alpha_n)]).\end{aligned} \tag{B1}$$

Using the change of variable

$$\Delta d_n = d_n - D - \kappa[\Delta R_\parallel(\alpha_{n-1}) + \Delta R_\parallel(\alpha_n)], \tag{B2}$$

the integration over d_n using Eq. (3.11) and the definition of σ_D gives

$$\begin{aligned}\sigma_{d_n}^2(\mathrm{SSCA}) &= \int\int p[\Delta R_\parallel(\alpha_{n-1})]p[\Delta R_\parallel(\alpha_n)] \\ &\quad\times\{\sigma_D^2 + \kappa^2[\Delta R_\parallel(\alpha_{n-1}) + \Delta R_\parallel(\alpha_n)]^2\} \\ &\quad\times d\Delta R_\parallel(\alpha_{n-1})d\Delta R_\parallel(\alpha_n).\end{aligned} \tag{B3}$$

As the sizes of two neighbors are not correlated this yields

$$\sigma_{d_n}^2(\mathrm{SSCA}) = \sigma_D^2 + 2\kappa^2\sigma_{R_\parallel}^2. \tag{B4}$$

In LMA with a spacing $d_n=D+2\kappa\Delta R_\parallel(\alpha_n)$ in each monodisperse domain, the calculation is analogous to the previous one. However, as the integration is over the domain of size $R_\parallel(\alpha_n)$, the final result reads

$$\sigma_{d_n}^2(\mathrm{LMA}) = \sigma_D^2 + 4\kappa^2\sigma_{R_\parallel}^2. \tag{B5}$$

*Corresponding author: remi.lazzari@insp.jussieu.fr
†leroy@crmcn.univ-mrs.fr
‡grenaud@cea.fr

[1] R. Lazzari, F. Leroy, G. Renaud, and J. Jupille, Phys. Rev. B **76**, 125412 (2007).
[2] J. A. Venables, Philos. Mag. **27**, 697 (1973).
[3] M. Zinke-Allmang, Thin Solid Films **346**, 1 (1999).
[4] A. Barabási and H. Stanley, *Fractal Concepts in Surface Growth* (Cambridge University Press, Cambridge, 1995).
[5] G. Renaud *et al.*, Science **300**, 1416 (2003).
[6] G. Renaud, M. Ducruet, O. Ulrich, and R. Lazzari, Nucl. Instrum. Methods Phys. Res. B **222**, 667 (2004).
[7] S. K. Sinha, E. B. Sirota, S. Garoff, and H. B. Stanley, Phys. Rev. B **38**, 2297 (1988).
[8] M. Rauscher, T. Salditt, and H. Spohn, Phys. Rev. B **52**, 16855 (1995).
[9] M. Rauscher, R. Paniago, H. Metzger, Z. Kovats, J. Domke, H. D. Pfannes, J. Schulze, and I. Eisele, J. Appl. Phys. **86**, 6763 (1999).
[10] A. Guinier and G. Fournet, *Small-angle Scattering of X-rays* (Wiley, New York, 1955).
[11] C. Vonk, J. Appl. Crystallogr. **9**, 433 (1976).
[12] J. S. Pedersen, J. Appl. Crystallogr. **27**, 595 (1994).
[13] W. Bertram, J. Appl. Crystallogr. **29**, 682 (1996).
[14] D. Gazzillo, A. Giacometti, R. Guido Della Valle, F. Venutti, and E. Carsughi, J. Chem. Phys. **111**, 7636 (1999).
[15] C. Revenant, F. Leroy, R. Lazzari, G. Renaud, and C. R. Henry, Phys. Rev. B **69**, 035411 (2004).
[16] R. Lazzari, J. Appl. Crystallogr. **35**, 406 (2002).
[17] N. Jedrecy, G. Renaud, R. Lazzari, and J. Jupille, Phys. Rev. B **72**, 045430 (2005).
[18] L. B. N. Laboratory, http://www-cxro.lbl.gov/
[19] D. K. G. de Boer, Phys. Rev. B **53**, 6048 (1996).
[20] A. Sentenac and J.-J. Greffet, J. Opt. Soc. Am. A **15**, 528 (1998).
[21] S. Dietrich and A. Haase, Phys. Rep. **260**, 1 (1995).
[22] D. K. G. de Boer, Phys. Rev. B **51**, 5297 (1995).
[23] C. Guérin and A. Sentenac, J. Opt. Soc. Am. A **21**, 1251 (2004).
[24] D. K. G. de Boer, Phys. Rev. B **44**, 498 (1991).
[25] D. Stearns, J. Appl. Phys. **65**, 491 (1989).
[26] V. Holý, J. Kubena, I. Ohlídal, K. Lischka, and W. Plotz, Phys. Rev. B **47**, 15896 (1993).
[27] V. Holý and T. Baumbach, Phys. Rev. B **49**, 10668 (1994).
[28] M. Kopecky, J. Appl. Phys. **77**, 2380 (1995).
[29] P. Mikulík and T. Baumbach, Phys. Rev. B **59**, 7632 (1999).
[30] K. Omote, Y. Ito, and S. Kawamura, Appl. Phys. Lett. **82**, 544 (2003).
[31] P. Busch, M. Rauscher, D.-M. Smilgies, D. Posselt, and C. M. Papadakis, J. Appl. Crystallogr. **39**, 433 (2006).
[32] G. Glatter and O. Kratky, *Small Angle X-ray Scattering* (Academic, London, 1982).
[33] R. Balescu, *Equilibrium and Nonequilibrium Statistical Mechanics* (Wiley, New York, 1975).
[34] Y. Waseda, *The Structure of Non-crystalline Materials* (McGraw-Hill, New York, 1980).
[35] A. Vrij, J. Chem. Phys. **69**, 1742 (1978).
[36] A. Vrij, J. Chem. Phys. **71**, 3267 (1979).
[37] P. Van Beurten and A. Vrij, J. Chem. Phys. **74**, 2744 (1981).
[38] J. S. Pedersen, Phys. Rev. B **47**, 657 (1993).
[39] J. Venables, *Introduction to Surface and Thin Film Processes* (Cambridge University Press, Cambridge, United Kingdom, 2000).
[40] A. Guinier, *X-ray Diffraction in Crystals, Imperfect Crystals and Amorphous Bodies* (Dover, New York, 1963).
[41] R. Hosemann and S. N. Bagchi, *Direct Analysis of Diffraction by Matter* (North-Holland, Amsterdam, 1962).
[42] M. Kotlarchyk and S.-H. Chen, J. Chem. Phys. **79**, 2461 (1983).
[43] D. Babonneau, F. Pailloux, J.-P. Eymery, M. F. Denanot, P. Guérin, E. Fonda, and O. Lyon, Phys. Rev. B **71**, 035430 (2005).
[44] B. E. Warren, *X-ray Diffraction* (Dover, New York, 1969).
[45] F. Leroy, R. Lazzari, and G. Renaud, Acta Crystallogr., Sect. A: Found. Crystallogr. **60**, 565 (2004).
[46] R. Hosemann, Acta Crystallogr. **4**, 520 (1951).
[47] R. Hosemann and A. Hindeleh, J. Macromol. Sci., Phys. **B34**, 327 (1995).
[48] R. Millane and J. Eads, Acta Crystallogr., Sect. A: Found. Crystallogr. **A56**, 497 (2000).
[49] G. H. Vineyard, Phys. Rev. B **26**, 4146 (1982).
[50] J. Daillant and A. Gibaud, *X-ray and Neutron Reflectivity: Principle and Applications*, Lectures Notes in Physics (Springer, New York, 1999).
[51] A. Caticha, Phys. Rev. B **62**, 3639 (2000).
[52] A. Messiah, *Quantum Mechanics* (Dunod, Paris, 1964), Vol. 1–2.
[53] J. S. Pedersen, P. Vysckocil, B. Schönfeld, and G. Kostorz, J. Appl. Crystallogr. **30**, 975 (1997).
[54] G. R. Carlow and M. Zinke-Allmang, Phys. Rev. Lett. **78**, 4601 (1997).
[55] G. Carlow, Physica A **239**, 65 (1997).
[56] P. A. Mulheran and J. A. Blackman, Phys. Rev. B **53**, 10261 (1996).
[57] B. Croset and C. de Beauvais, Surf. Sci. **384**, 15 (1997).
[58] B. Croset and C. de Beauvais, Surf. Sci. **409**, 403 (1998).
[59] S. Pflanz and W. Moritz, Acta Crystallogr., Sect. A: Found. Crystallogr. **48**, 716 (1992).
[60] H. Matsuoka, H. Tanaka, T. Hashimoto, and N. Ise, Phys. Rev. B **36**, 1754 (1987).
[61] H. Matsuoka, H. Tanaka, N. Iizuka, T. Hashimoto, and N. Ise, Phys. Rev. B **41**, 3854 (1990).
[62] X.-Q. Mu, Acta Crystallogr., Sect. A: Found. Crystallogr. **54**, 606 (1998).
[63] J. Eads and R. Millane, Acta Crystallogr., Sect. A: Found. Crystallogr. **57**, 507 (2001).